JOURNAL OF MATERIALS SCIENCE 28 (1993) 2923–2932

Tensile properties and inhomogeneous deformation of ferrite–martensite dual-phase steels

THAK SANG BYUN, IN SUP KIM
Department of Nuclear Engineering, Korea Advanced Institute of Science and Technology, Kusongdong 373-1, Yusunggu, Daejon 305-701, Korea

The tensile properties and inhomogeneous deformation of coarse ferrite–martensite dual-phase steels containing 17–50% martensite were analysed. The stress of dual-phase steels at equal strain increased with increasing volume fraction of martensite, f, but the rate of increase was reduced after $f = 0.3$. The strain hardening rate was dependent on f at small strains ($\varepsilon \leqslant 0.03$), however, it became independent of f at larger strains. It was found that the deformation of the dual-phase steels divided into three different stages when f was less than about 0.3. The concurrent *in situ* stress–strain states of ferrite, martensite and their composite, and the stress ratios and strain ratios between ferrite and martensite were evaluated by means of a new stress and strain partition theory. The martensite phase deformed plastically after the uniform strain for $f < 0.25$, while it was plastic before the uniform strain for $f > 0.25$. The theoretical analyses for inhomogeneous deformation implied that the volume-fraction dependence of the stress and the characteristics of the strain-hardening rate were influenced by the plastic deformation of martensite. Further, the *in situ* stress–strain curves of ferrite and martensite and the internal stresses at respective phases were calculated from the partitioned stresses and strains.

1. Introduction

Dual-phase steels are composite materials consisting of a soft ferrite matrix and hard martensite particles, which are produced by intercritical annealing followed by accelerated cooling [1–3]. If an external force is applied to the ferrite–martensite composite, the mechanical interactions arising from the constraints between the two different phases bring about inhomogeneous distributions of stress and strain [4–8]. The mechanical behaviours of dual-phase steels arise from the processes of stress and strain partition between constituent phases. Yet, there are few systematic descriptions of the inhomogeneous deformation and the relationships between the macroscopic mechanical properties and the inhomogeneous deformation. The objectives of the present study are to analyse the inhomogeneous deformation of dual-phase steels systematically, and to find relationships between tensile properties and the stress and strain partition.

Various types of inhomogeneous deformation were observed in dual-phase steels [6–7]. If a dual-phase steel contained a small amount of high-carbon martensite, only the ferrite phase deformed plastically, so the stress and strain partition was similar to that of particle-hardened alloys [9–13]; however, if the steel included a large amount of ductile martensite, the stress and strain partition was similar to that of duplex alloys containing two plastically deformable phases [13–14]. Further, the inhomogeneous deformation of ferrite–martensite dual-phase steels may include various phenomena such as plastic deformation of ferrite, accumulation of unrelaxed plastic incompatibility [15–21], plastic relaxation [22–26] and yielding of martensite [7, 14].

The authors [13] have developed a stress- and strain-partition theory using the Lagrangian-multiplier method, by which the elastic and plastic deformations in alloys such as WC–Co, spheroidized carbon steel, and duplex stainless steel were successfully analysed. In this work the theory is modified, as detailed in the Appendix, and the modified theory is used to calculate the stress and strain partition in dual-phase steels containing various volume fractions of martensite. Also, the tensile-deformation properties of the ferrite–martensite composites are analysed in terms of the volume-fraction dependence of stress and the variation of the strain-hardening rate. Then an explanation is given for the macroscopic mechanical behaviour by means of the theoretically calculated results for stress and strain inhomogeneity.

2. Material and experimental procedures

The material for this investigation was manufactured as billet, and the chemical composition of the material was Fe–0.11 wt % C–1.64 wt % Mn–0.78 wt % Si. The billet was hot extruded forming rods of 20 mm diameter, and then the rods were machined to round tensile specimens of 8 mm diameter and 45 mm gauge

0022–2461

length. The tensile specimens, having various volume-fractions of ferrite and martensite, were prepared by the heat-treatment schedules shown in Fig. 1. Each heat-treatment schedule consisted of austenitization at 930 °C for 30 min and water quenching at various intercritical temperatures between 660 °C and 930 °C during cooling at a rate of 100 °C h^{-1}.

Metallographic specimens were etched in a meta-bisulphite solution, which revealed microstructures of white-ferrite–dark-martensite. The volume fractions of constituent phases were determined by a point-counting method on micrographs (Fig. 2). Further, mean intercept lengths of the ferrite and martensite were measured on the micrographs.

Tensile tests were performed at room temperature in a universal testing machine with a strain rate of $1.67 \times 10^{-4}\,s^{-1}$. The true-stress–true-strain curves were calculated from records of load and displacement. Vickers microhardness numbers, H_V, of ferrite and martensite were measured on the etched surfaces of the round tensile specimens which were deformed by the uniform strain.

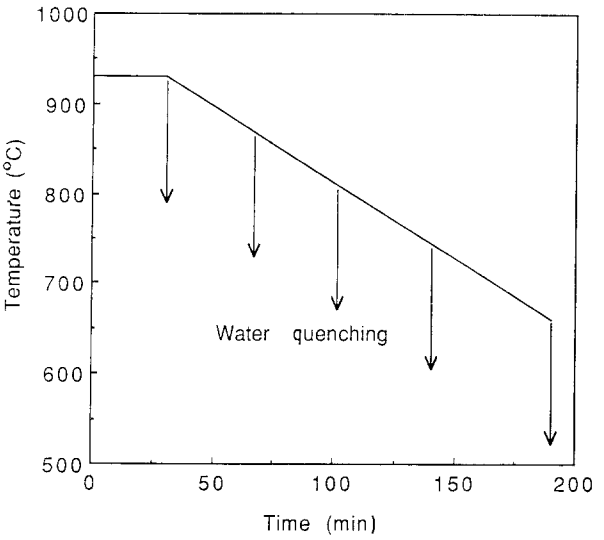

Figure 1 Heat-treatment schedules to produce various ferrite–martensite dual-phase steels. The cooling rate is 100 °C h^{-1}.

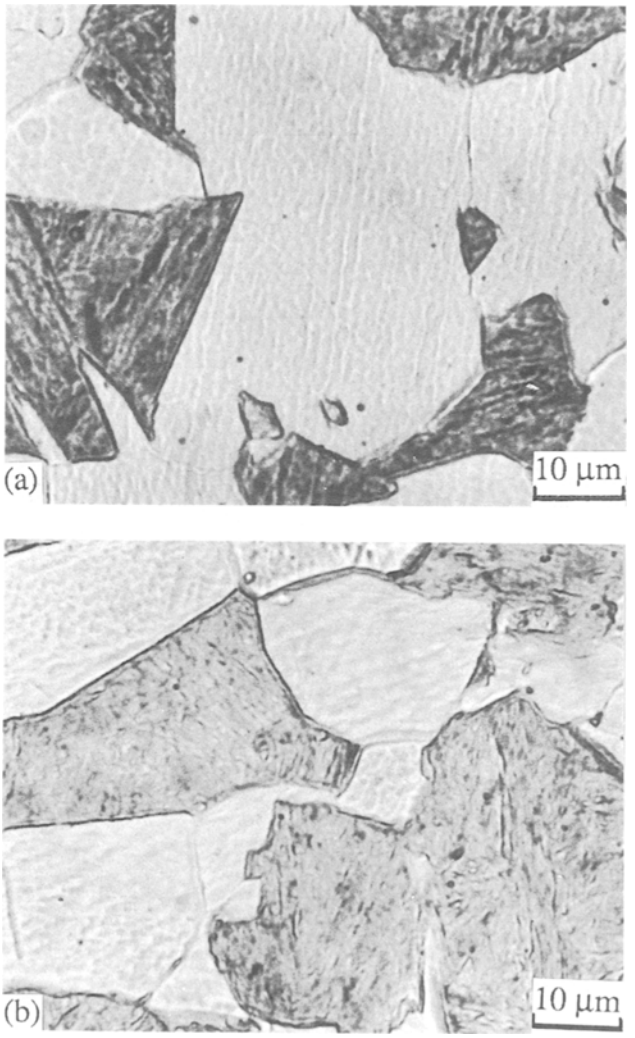

Figure 2 Optical micrographs of coarse-grained ferrite–martensite dual-phase steels. The dark is martensite phase and the white is ferrite phase (etched in metabisulphite solution). Volume fractions of martensite: (a) 0.24, and (b) 0.5.

3. Calculation method for the stress and strain partition of dual-phase steels

3.1. Calculation of stress and strain partition

The governing equations for the inhomogeneous deformation of two-phase alloys have been derived by the authors [13] using a Lagrangian-multiplier method. In the present work the authors' theory [13] is modified in the Appendix, and the modified theory is applied to inhomogeneous deformation of dual-phase steels.

Tomota *et al.* [14] classified the inhomogeneous deformation of two-phase alloys into three stages. In stage A both phases deform elastically. In stage B the soft phase deforms plastically while the hard phase remains in the elastic state. Finally, in stage C both phases deform plastically. The calculation procedures for these three stages were designed as follows.

In stage A, since both ferrite and martensite in dual-phase steels have the same elastic constants, the deformation was assumed to be homogeneous. The elastic modulus of the ferrite and martensite, E, was assumed to be 207 GPa.

In stage B, the martensite phase deforms elastically. The constitutive equation for the elastic martensite can be given by

$$\sigma_2 = E\varepsilon_2 = 207\varepsilon_2 \quad \text{(GPa)} \qquad (1)$$

Note that the subscripts 1 and 2 to stress, σ, and strain, ε, denote ferrite and martensite, respectively. The Hollomon-type stress–strain curves [33] of the ferrite–martensite composites are of the form $\sigma = K\varepsilon^n$, where K is the strength coefficient and n the strain-hardening coefficient, and they can be given by the tensile experiments. As a result, two stress–strain relations are known for the martensite phase and for the composite. The governing equation for this stage is obtainable from Equation A15 as

$$(\sigma - \sigma_2)\varepsilon + \sigma(\varepsilon - \varepsilon_2) = 0 \qquad (2)$$

Equations 1 and 2 give the *in situ* effective strain of

martensite

$$\varepsilon_2 = \frac{2\sigma\varepsilon}{E\varepsilon + \sigma} \quad (3)$$

Then the *in situ* effective stress of martensite is given by

$$\sigma_2 = E\varepsilon_2 = \frac{2E\sigma\varepsilon}{E\varepsilon + \sigma} \quad (4)$$

Using the modified rules of mixtures represented by Equations A4 and A5 and using Equations 3 and 4, the *in situ* effective stress and *in situ* effective strain of the ferrite phase are obtained as

$$\sigma_1 = \frac{(E\varepsilon + \sigma - 2fE\varepsilon)\sigma}{(1-f)(E\varepsilon + \sigma)} \quad (5)$$

$$\varepsilon_1 = \frac{[E\varepsilon + (1-2f)\sigma]\varepsilon}{(1-f)(E\varepsilon + \sigma)} \quad (6)$$

These two equations give the *in situ* stress–strain curves of ferrite in stage B.

Finally, in stage C the martensite as well as the ferrite deforms plastically. According to the calculated results for the deformation of stage B, the *in situ* plastic-flow curve of ferrite was insensitive to the volume fraction of martensite. Therefore, the ferrite-flow curve for $f = 0.27$, which was calculated by Equations 5 and 6, was also used in all calculations for $f > 0.27$. The flow curve of the *in situ* ferrite phase is given by

$$\sigma_1 = 700\varepsilon_1^{0.13} \text{ (MPa)} \quad (7)$$

The governing equation at this stage is

$$(\sigma - \sigma_1)\varepsilon + \sigma(\varepsilon - \varepsilon_1) = 0 \quad (8)$$

With two flow curves, $\sigma = K\varepsilon^n$ for a ferrite–martensite composite and $\sigma_1 = K_1\varepsilon_1^{n_1}$ for ferrite, Equation 8 was solved by a bisection iterating method. The partitioned stresses and strains of the martensite phase were also calculated from the calculated stresses and strains of the composite and ferrite phase by means of the modified rules of mixtures (Equations A4 and A5).

3.2. Calculation of internal stresses and stress and strain components

In this paper the internal stress (long range) was defined by the stress difference between the average stress of a composite and the average stress of each phase. If it is assumed that martensite particles are randomly oriented in the ferrite matrix and that an external stress, σ ($= \sigma_{11}$), is applied to a composite body in the uniaxial direction of 11, the relations between the internal-stress components of the tensile direction (11) and transverse directions (22 and 33) are given by [9, 14]

$$\sigma_{22}^{1I} = \sigma_{33}^{1I} = -\tfrac{1}{2}\sigma_{11}^{1I} \quad (9)$$

$$\sigma_{22}^{2I} = \sigma_{33}^{2I} = -\tfrac{1}{2}\sigma_{11}^{2I} \quad (10)$$

where the superscripts 1I and 2I denote the internal stresses at phase 1 and phase 2, respectively. Any shear component is zero. Then, the stress components for the 11, 22 and 33 directions at each phase become

$$\sigma_{11}^1 = \sigma + \sigma_{11}^{1I} \quad (11)$$

$$\sigma_{11}^2 = \sigma + \sigma_{11}^{2I} \quad (12)$$

$$\sigma_{22}^1 = \sigma_{33}^1 = -\tfrac{1}{2}\sigma_{11}^{1I} \quad (13)$$

$$\sigma_{22}^2 = \sigma_{33}^2 = -\tfrac{1}{2}\sigma_{11}^{2I} \quad (14)$$

Here the superscripts 1 and 2 indicate the ferrite and martensite phase, respectively. Using Equations 9–14 and the definition of effective stress, the effective stresses at ferrite and martensite, σ_1 and σ_2, are derived as

$$\sigma_1 = \frac{1}{2^{1/2}}[(\sigma_{11}^1 - \sigma_{22}^1)^2 + (\sigma_{22}^1 - \sigma_{33}^1)^2 + (\sigma_{33}^1 - \sigma_{11}^1)^2]^{1/2} = \sigma + \tfrac{3}{2}\sigma_{11}^{1I} \quad (15)$$

$$\sigma_2 = \frac{1}{2^{1/2}}[(\sigma_{11}^2 - \sigma_{22}^2)^2 + (\sigma_{22}^2 - \sigma_{33}^2)^2 + (\sigma_{33}^2 - \sigma_{11}^2)^2]^{1/2} = \sigma + \tfrac{3}{2}\sigma_{11}^{2I} \quad (16)$$

Therefore, the 11 components of internal stress at respective phases are given by

$$\sigma_{11}^{1I} = \tfrac{2}{3}(\sigma_1 - \sigma) \quad (17)$$

$$\sigma_{11}^{2I} = \tfrac{2}{3}(\sigma_2 - \sigma) \quad (18)$$

Additionally, it is assumed that the effective strains, ε_1, ε_2 and ε, and components of the total strains, elastic strains plus plastic strains, were interrelated by [13]

$$\varepsilon_{22}^1 = \varepsilon_{33}^1 = -\tfrac{1}{2}\varepsilon_{11}^1 = -\tfrac{1}{2}\varepsilon_1 \quad (19)$$

$$\varepsilon_{22}^2 = \varepsilon_{33}^2 = -\tfrac{1}{2}\varepsilon_{11}^2 = -\tfrac{1}{2}\varepsilon_2 \quad (20)$$

$$\varepsilon_{22} = \varepsilon_{33} = -\tfrac{1}{2}\varepsilon_{11} = -\tfrac{1}{2}\varepsilon \quad (21)$$

where the subscripts 11, 22 and 33 also denote the components of strain, and the superscripts 1 and 2 the respective phases.

4. Results and discussion

4.1. Microstructure of ferrite–martensite dual-phase steels

Representative micrographs of coarse dual-phase steels are illustrated in Fig. 2. In these microstructures martensite islands (dark phase) of irregular shape are embedded in the continuous ferrite phase. Since the ferrite phase had primarily nucleated at the austenite grain boundaries and grown into the interior of the austenite grain during cooling in the region of intercritical temperature [27], the ferrite phase became a continuous phase after water quenching, and so it is regarded as the matrix phase in ferrite–martensite composites. The contiguity of martensite, however, increases as its volume fraction increases [28].

The effect of the quenching temperature on the volume fraction of martensite is presented in Table I. The ferrite phase was rarely transformed from the austenite phase until the temperature of the specimens reached about 800 °C during cooling from austenitization at 930 °C (the martensite content of the specimen quenched from 800 °C was about 95%). But the austenite phase

TABLE I Variation of martensite-volume fraction and summary of tensile test results: YS is the 0.2% offset yield stress, and UTS the ultimate tensile stress

Quenching temperature T (°C)	f	K (MPa)	n	YS (MPa)	UTS (MPa)
660	0.17	1296	0.245	312	767
680	0.22	1245	0.220	331	797
700	0.24	1246	0.199	387	802
710	0.27	1254	0.183	395	839
720	0.32	1305	0.185	393	865
730	0.37	1288	0.162	395	904
740	0.43	1298	0.157	482	919
750	0.50	1311	0.150	440	945

transformed rapidly into the ferrite phase between 800 and 700 °C. The minimum amount of untransformed austenite, which became martensite after quenching, was about 17%.

4.2. Strength of dual-phase steels and strain-hardening characteristics

Table I also contains the Hollomon constants, strength coefficient, K, and strain-hardening coefficient, n, and 0.2% offset yield stress (0.2% YS) and ultimate tensile stress (UTS) for various volume-fractions of martensite. The Hollomon curves were fitted from the true-stress–true-strain curves of dual-phase steels. K is rarely influenced by f; however, n decreases as f increases. This fact implies that the strain-hardening rate at early deformation increases as f increases.

Fig. 3 shows the stresses as functions of martensite content. With the exception of small strains ($\varepsilon \leqslant 0.01$), the stress at each strain increases with increasing volume fraction of martensite. A transition in the slopes, $d\sigma/df$, appears at $f = 0.3$; the slopes in the range $0.17 \leqslant f \leqslant 0.27$ are approximately three times as large as those in the range $0.32 \leqslant f \leqslant 0.50$. In contrast, the UTS in Table I did not reveal a transition point; the volume-fraction dependence of UTS was given by a well-fitted curve: UTS = 677 + 564f(MPa).

Strain-hardening rates, $d\sigma/d\varepsilon$, were calculated from the experimental stress–strain curves, and they are represented in Fig. 4 as $\log(d\sigma/d\varepsilon) - \log(\varepsilon)$ plots. The description of strain-hardening behaviour using the $\log(d\sigma/d\varepsilon) - \log(\varepsilon)$ plot is called Jaoul–Crussard analysis [29]. This figure shows that the slope of the strain-hardening rate has three different stages. This means the deformation is divided into three stages; I, II and III. Stage I is the deformation before a strain of about 0.007; stage II is strain in the range 0.007–0.03; and strains larger than 0.03 are contained in stage III. As seen in Fig. 4 the strain hardening rate in the stages I and II is proportional to the volume-fraction of martensite, f, while in stage III it is almost independent of martensite content.

Lawson *et al.* [3] also observed three different stages in the Jaoul–Crussard plots of dual-phase steels. According to their results, when a small amount of martensite was contained in dual-phase steel, three

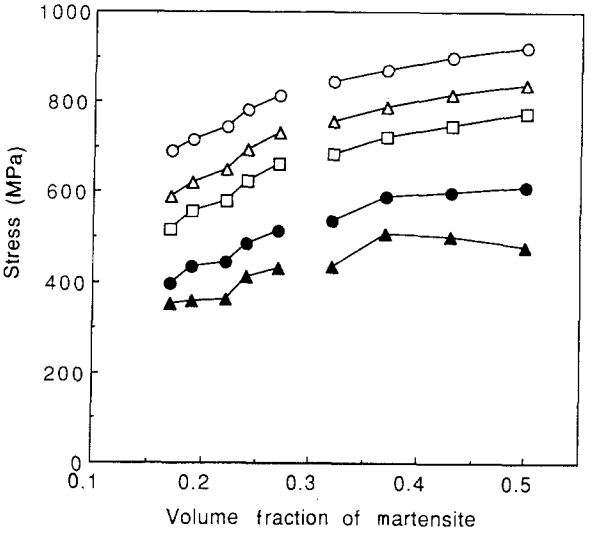

Figure 3 Volume-fraction dependence of stress at several strains: (○) 0.10, (△) 0.05, (□) 0.03, (●) 0.01, and (▲) 0.005.

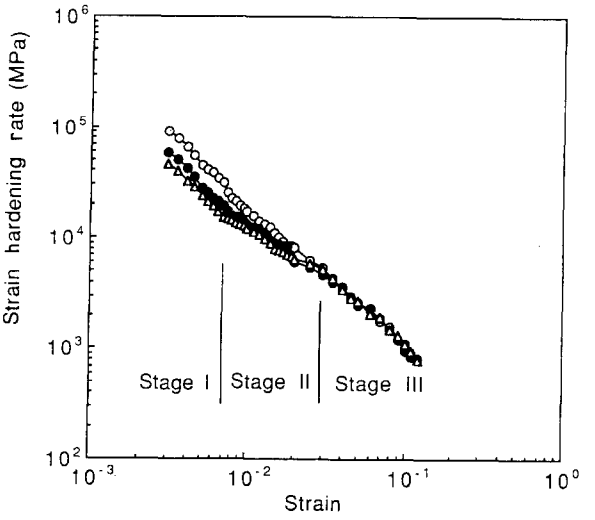

Figure 4 Strain-hardening rate as a function of strain. Deformation is divided into three stages by the strains at 0.007 and 0.03. The strain-hardening rates are shown for three values of f: (○) 0.50, (●) 0.27, and (△) 0.24.

deformation stages clearly appeared in the Jaoul–Crussard plot. However, the Jaoul–Crussard plot for $f = 0.34$ appeared as a straight line, so the stress–strain curve was drawn by a single parabolic curve. According to the results of the present work and to Lawson *et al.* the three-stage deformation, which seems to come from the characteristics of deformation of a body-centred cubic (b.c.c.) ferrite phase, disappears when the martensite content in the dual-phase steel is larger than about 30%. The transitions shown in Fig. 3 also occur at $f = 0.3$. These transitions will be explained by the stress and strain partition described in the following sections.

4.3. Inhomogeneous deformation of dual-phase steels

Stress and strain partitions are represented in Figs 5 and 6 by relating the stress–strain curves of the *in situ* ferrite; σ_1–ε_1, *in situ* martensite; σ_2–ε_2, and their composite;

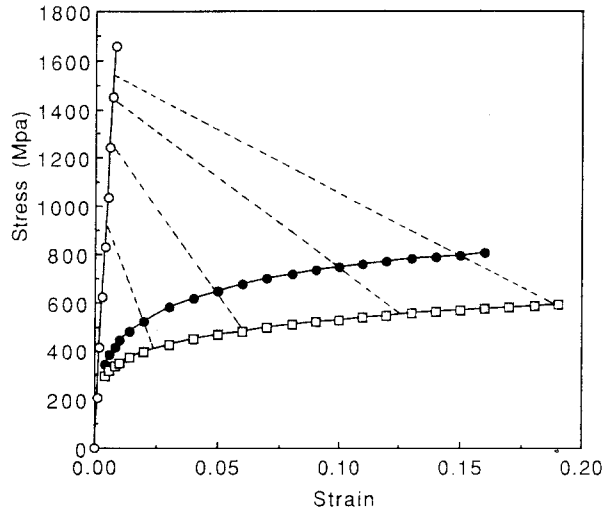

Figure 5 Relations between the *in situ* stress–strain curves of: (□) ferrite, (○) martensite, and (●) their composite when martensite ($f = 0.22$) has no plasticity. The concurrent stress–strain states are related by dashed tie lines at $\varepsilon = 0.02$, 0.05, 0.10 and 0.15.

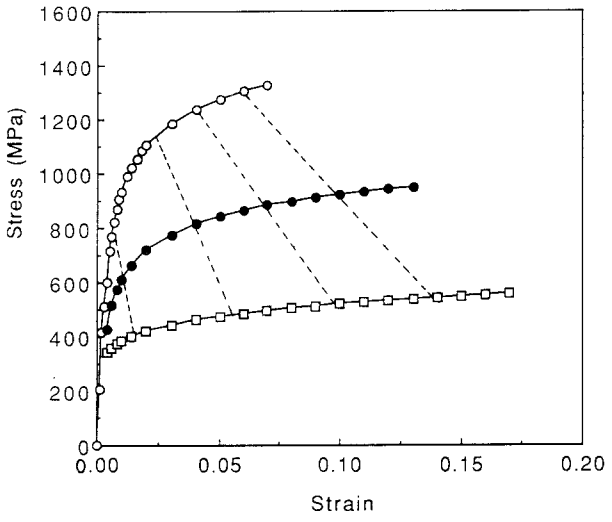

Figure 6 Relations between the *in situ* stress–strain curves of: (□) ferrite, (○) martensite, and (●) their composite when martensite ($f = 0.50$) has large plasticity. The concurrent stress–strain states are related by the dashed tie lines at $\varepsilon = 0.01$, 0.04, 0.07 and 0.10.

σ–ε. Fig. 5 shows the stress and strain partition in a dual-phase steel containing a relatively small amount of high-strength martensite ($f = 0.22$). In this case the martensite phase deforms elastically during most of the deformation range. This case is very similar to the spheroidized carbons steels [9–12]. According to the classification of Tomota *et al.* [14] (classification for deformation stages), the deformation of Fig. 5 is in stage B. The dashed lines indicate $\varepsilon = 0.02$, 0.05, 0.10 and 0.15, and they connect the concurrent stress–strain states of the *in situ* ferrite, martensite and composite. If the dashed line is parallel to the stress axis, it corresponds to an iso-strain theory, and if the dashed line is parallel to the strain axis, it corresponds to an iso-stress theory. The dashed lines in Fig. 5 are between the iso-strain and the iso-stress lines. Therefore, the theory used in this work is an intermediate theory between iso-strain and iso-stress theory [13].

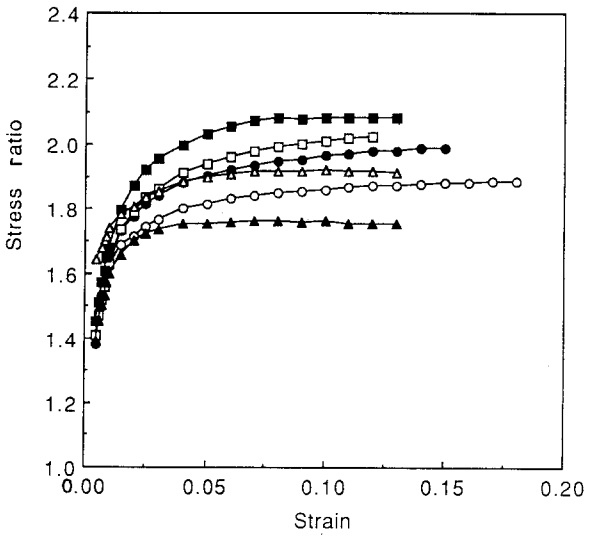

Figure 7 Variation of stress ratios between martensite and ferrite during deformation, for various values of f: (○) 0.17, (●) 0.22, (□) 0.24, (■) 0.27, (△) 0.37, (▲) 0.50.

Fig. 6 shows the relation between the *in situ* stress–strain curves of the ferrite, martensite and their composite for $f = 0.5$. The martensite phase is plastically deformable after about 1% composite strain, so the deformation becomes the third stage of the classification of Tomota *et al.* for deformation. The dashed tie lines (connecting corresponding partitioned stresses and strains of ferrite, martensite and dual-phase steel) are marked at strains 0.01, 0.04, 0.07 and 0.10. One can observe that large amounts of martensite ($f = 0.5$) induce large plastic deformation of the martensite itself.

Fig. 7 represents the variation of stress ratios, $\sigma^2_{11}/\sigma^1_{11}$, during straining. The stress ratios in the dual-phase steels increased rapidly from 1.0 during early deformation and were nearly saturated after about 5% strain. With the exception of the small strain region, the stress ratios were between 1.6 and 2.2. By using the shear-lag model. Szewczyk and Gurland [6] showed that the stress ratio was 2.25 for a dual-phase steel with $f = 0.16$. Further, the stress ratio from the back stress data of Gerbase *et al.* [5] for a dual-phase steel with $f = 0.15$ was 2.3 at 1% strain [6]. The stress ratio increases as the martensite content increases, but after $f = 0.3$ it decreases. This is because the martensite phase becomes softer as its volume-fraction increases. Reduction in the strength of martensite (austenite before quenching) is mainly caused by the reduction of the carbon concentration of martensite. Note that the average carbon content is 0.11 wt %, but almost all of the carbon atoms stay preferentially in the austenite phase at intercritical temperature.

Fig. 8 shows the variation of the microhardness numbers of ferrite and martensite. The experimental data were measured in specimens strained by the uniform strain. The specimen surface for the microhardness test was perpendicular to the tensile direction, so the indentation direction was parallel to the tensile directon. The calculated values were obtained from the 11-components of partitioned stresses at the uniform strains of respective dual-phase steels by using

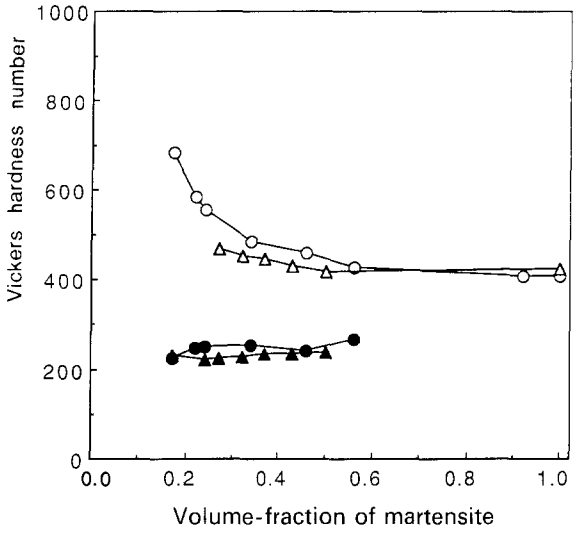

Figure 8 Vickers microhardness numbers of ferrite and martensite as the functions of the volume-fraction of martensite. The theoretically calculated values are compared with the experimental data: (△) martensite theoretical value, (▲) ferrite theoretical value, (○) martensite experimental value, and (●) ferrite experimental value.

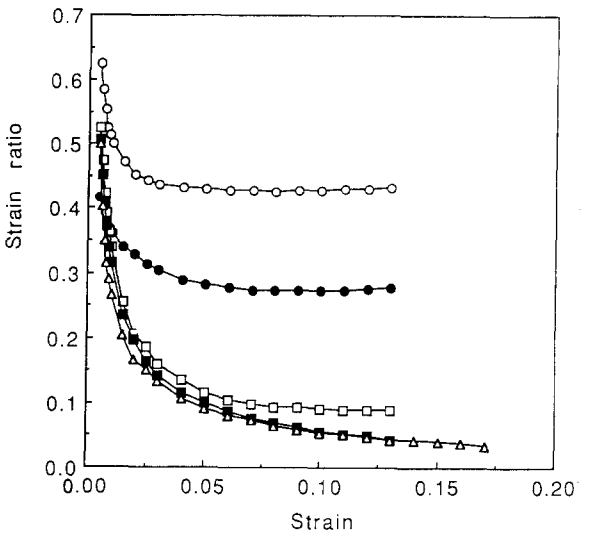

Figure 9 Variation of strain ratios between martensite and ferrite during deformation, for various values of f: (○) 0.50, (●) 0.37, (□) 0.27, (■) 0.24, and (△) 0.17.

the following equation [30]

$$\sigma_{11}^1 = 2.9H_V^1 \quad \text{(MPa)} \tag{22}$$

$$\sigma_{11}^2 = 2.9H_V^2 \quad \text{(MPa)} \tag{23}$$

where H_V^1 and H_V^2 denote the Vickers microhardness numbers of ferrite and martensite, respectively. For both phases the measured and the theoretical values agree. In Fig. 8, the strength of martensite decreases rapidly until martensite-volume fraction reaches about 30%, and then it has little variation even if the volume fraction of martensite increases greatly. The strength of ferrite, however, is preserved although martensite content increases. The microhardness ratios between plastically deformed martensite and ferrite have values between 1.6 and 2.2, which coincide with the stress ratios in Fig. 7. Our conclusion is that the present theory describes the stress partition well.

The variation of strain ratios, $\varepsilon_{11}^2/\varepsilon_{11}^1$, is sensitive to the volume fraction and strength of the martensite phase, as seen in Fig. 9. The strain ratio for small f decreases rapidly during early deformation, and it becomes smaller at larger strain. This is because the strength of martensite is so high that the martensite phase has no plasticity. However, as the martensite content in dual-phase steel increases, the martensite may deform plastically from small strain, then the strain ratio increases rapidly. This may be caused by reduction of the strength of martensite due to the dilution of the carbon concentration in martensite (austenite before quenching). The strain ratio for $f = 0.5$ decreases rapidly from 1.0 during early straining, but it increases slightly after about 5% strain. This increase may come from the plastic deformation of martensite.

Shen *et al.* [7] observed the inhomogeneous deformation of dual-phase steels, and concluded that the strain ratio, which defines the degree of strain inhomogeneity, depends on the microstructural parameters; it increases with increasing volume fraction of martensite, but decreases as the carbon content of the martensite increases. They also showed that tempering caused an increase in the strain ratio. It was also proved that the stress ratio increased as f increased if the strength of the second phase did not vary [13]. Therefore, one can conclude that the degree of stress and strain inhomogeneity in dual-phase steels is mainly determined by the volume-fraction and strength of martensite.

TABLE II Variation of carbon content in ferrite and martensite and yield stress σ_{YS} of martensite. The average carbon content of the steel is 0.11 wt %.

f	C_1 (wt %)	C_2 (wt %)	σ_{YS}^2 (MPa)
0.17	0.0114	0.5914	2224
0.22	0.0142	0.4497	1843
0.24	0.0170	0.4045	1722
0.27	0.0184	0.3577	1596
0.32	0.0198	0.3017	1446
0.37	0.0218	0.2601	1334
0.43	0.0206	0.2285	1249
0.50	0.0194	0.2006	1174

4.4. Initiation of plastic deformation of martensite and tensile properties

The theoretically calculated composite strain at which the martensite phase began to deform plastically was compared with the uniform strain of the composite (dual-phase steel). The 0.2% offset yield stress of martensite was calculated by the relation given by Leslie [31]:

$$\sigma_{YS}^2 = 635 + 2687C_2 \quad \text{(MPa)} \tag{24}$$

where C_2 is the carbon content at the martensite phase in wt %. As the average carbon content of the present dual-phase steels was 0.11 wt %, C_2 was obtained by the following relation

$$C_2 = \frac{0.11 - (1 - f)C_1}{f}. \tag{25}$$

The equilibrium carbon content of the ferrite phase, C_1, was obtained from the equilibrium phase diagram of Fe–C system [32]. The strain at which martensite yields was determined by the macroscopic strain at which the partitioned effective stress of martensite, σ_2, reached the calculated value of σ_{YS}^2.

As shown in Fig. 10, the strain for martensite yield decreases rapidly as the volume fraction of martensite increases to about 30%, while the uniform strain decreases slowly. The two curves intercept at $f = 0.25$. This means that the martensite phase yields after uniform strain when the martensite content is less than about 25%, but it deforms plastically before uniform strain with a larger amount of martensite.

The transition at $f = 0.3$ in the increasing rate of composite stress shown in Fig. 3 can be explained by means of the variation of the strain for martensite yield in Fig. 10. The martensite phase which is deforming elastically can more effectively bear loads, thus the value of $d\sigma/df$ is larger at small f than at large f. As f exceeds 0.3, the strength of martensite is reduced by dilution of the carbon content, so the martensite phase undergoes plastic deformation from early straining. The plastically deforming martensite sustains less stress than rigid high-carbon martensite because the unrelaxed incompatibility giving stress concentrations on martensite is relaxed by the plastic deformation of martensite.

The three stage deformation in Fig. 4 evidently arises from the deformation of ferrite [3], and it appears in the specimens containing a small amount of martensite phase ($f < 0.3$). However, as the amount of martensite increases above 0.3, the deformation is contained in stage C of the classification of Tomota *et al.* [14] from early deformation, and a large portion of total plasticity is attributed to the plasticity of martensite. The strain hardening in stage C may be characterized by combined effects from the strain hardening of ferrite and martensite. Then the three stages I, II and III in the strain-hardening rate become roughly a single stage as f increases above 0.3, because of the plastic deformation of martensite. It was concluded that the three stage deformation appears when plastic deformation of ferrite predominates over plastic deformation of the ferrite–martensite composite.

4.5. *In situ* stress–strain curves of ferrite and martensite

The ferrite and martensite in dual-phase steels constrain each other during deformation. Dislocation density as well as dislocation-slip mechanisms may be affected by the constraint effects. Ashby's strain-hardening theory [22–23] showed that the plastically deforming matrix was hardened by two short-range internal stresses: the hardening stress due to the statistically stored dislocations and the forest-hardening stress by the geometrically necessary dislocations. He assumed full relaxation of internal stresses caused by strain incompatibility. In addition to these two hardening stresses, Chang and Asaro [10] took into account, in their work-hardening model, the source shortening stress arising from the interactions between bowing dislocations and the stress field around hard particles. The hardening stress of the matrix phase due to the geometrically necessary dislocations and the source shortening stress are caused by the second phase. Therefore, the *in situ* stress–strain curve of the ferrite phase is different from the curve of ferrite which is free from martensite.

The *in situ* stress–strain curves were calculated by the method described in Section 3.1. The calculated *in situ* stress–strain curves of ferrite for several volume-fractions of martensite are plotted in Fig. 11. For low deformation, the strain hardening of the ferrite matrix increases as f increases. But the curves converge to a single curve after several percent strain. The difference between the strain-hardening rates of ferrite at low deformation can be explained by the variation of the size of ferrite due to the increase of martensite. Fig. 12 is the variation of the mean intercept lengths of each phase. Ashby's strain-hardening theory [22–23]

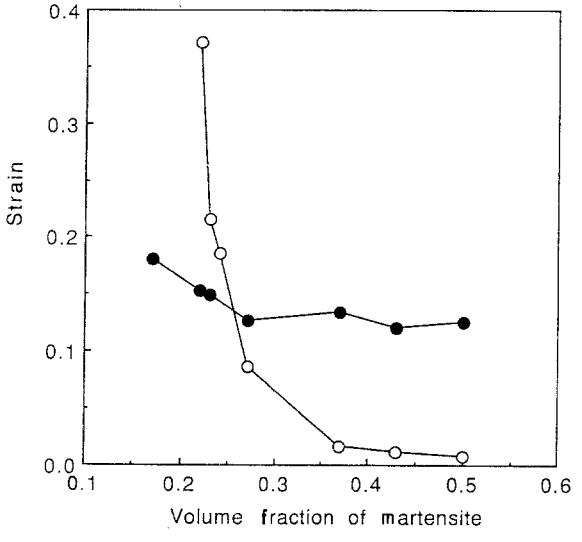

Figure 10 Comparison between: (●) the uniform strain, and (○) the composite strain, for martensite yield.

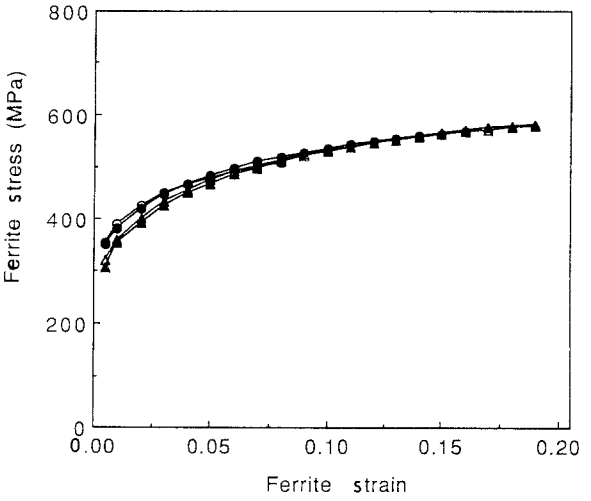

Figure 11 *In situ* stress–strain curves of the ferrite matrix in the elastic region of martensite, for various values of f: (○) 0.27, (●) 0.24, (△) 0.23, and (▲) 0.22.

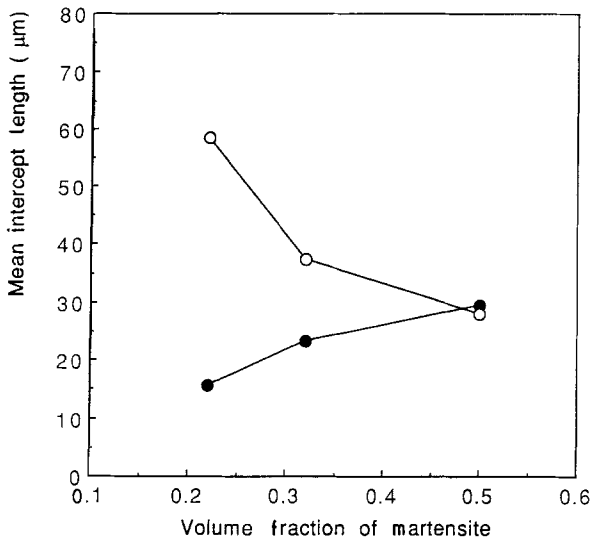

Figure 12 Mean intercept lengths as functions of the volume fraction of martensite, for: (●) martensite, and (○) ferrite.

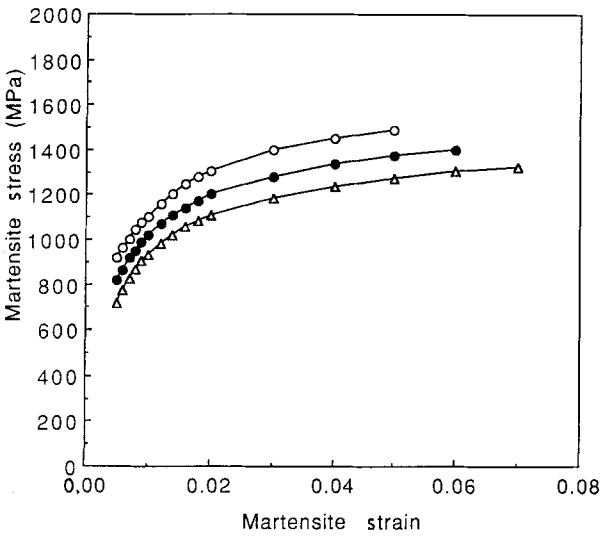

Figure 13 In situ stress–strain curves of the martensite phase in the plastic region of martensite, for various values of f: (○) 0.37, (●) 0.43, and (△) 0.5.

implies that the strain-hardening stress caused by the second phase is proportional to $(\lambda^G)^{-1/2}$, where λ^G was defined as the geometric slip distance, and was a characteristic of the microstructure. It should be noted that λ^G in a multiphase system of ferrite and martensite is proportional to the mean intercept length. Since the mean intercept length of the ferrite phase decreases with increasing volume fraction of martensite, as seen in Fig. 12, the ferrite stress at low deformation increases with martensite content. Also it was found that the hardening stress of the ferrite matrix due to the second phase increases at small strain and in the fine microstructures [23]. Since the specimens in this study have coarse microstructures, the phase-size dependence of the *in situ* stress–strain curves of ferrite disappears at large strains.

The *in situ* stress–strain curves of martensite, however, were obtained by the method described in Section 3.1., when the martensite phase deformed plastically. Fig. 13 includes the *in situ* stress–strain curves of martensite. The martensite strength decreases as the volume fraction of martensite increases. This fact may be because of the softening of the martensite phase by dilution of carbon content.

4.6. Internal stress development during deformation

Internal stress (long range) arises from unrelaxed plastic incompatibility. Unrelaxed plastic incompatibility is generated as the forms of Orowan dislocation loops accumulate around second-phase particles after the passing of dislocations [15], or accumulated dislocations are obstructed by large second-phase barriers. The development of unrelaxed plastic incompatibility is a process of load transfer from the ferrite matrix to martensite islands, and it is related to the stress partition between ferrite and martensite.

The 11-components of the internal stresses of respective phases can be calculated using Equations 17 and 18, and they are represented in Fig. 14. The absolute value of the internal stress in the ferrite matrix is

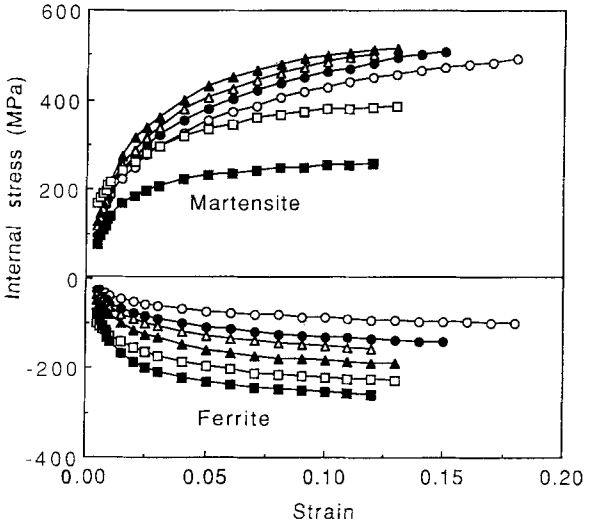

Figure 14 Variation of internal stresses at ferrite and martensite during straining, for various values of f: (○) 0.17, (●) 0.22, (△) 0.24, (▲) 0.27, (□) 0.37, and (■) 0.50.

called the back stress. Since the internal stress of ferrite is negative, the generation of the internal stress delays the further deformation of ferrite. Averages of internal stress over the composite volume are zero, thus for $f = 0.5$ the internal stresses of ferrite and martensite are equal.

The absolute values of the internal stresses at respective phases increase rapidly for low deformation; however, the rate of increase is much lower for greater deformation. The rate of increase of internal stress is influenced, at first, by the amount of plastic relaxation [18, 22–26]. As deformation proceeds to higher strain, the ferrite–martensite composite cannot accommodate the unrelaxed plastic incompatibility without plastic relaxation or crack formation, so plastic relaxation occurs to reduce internal stress which is too large to be sustained. Even with a small-volume fraction of the second phase, plastic relaxation occurs before 1%

strain [4, 18]. Most of the unrelaxed plastic incompatibility is relaxed by the formation of secondary dislocation loops [24–25] after a critical strain. But the plastic incompatibility of the unrelaxed state, which is a very small proportion of total strain, causes a significant amount of internal stress as illustrated in Fig. 14.

Another cause of the reduction of internal stress is plastic deformation of martensite. The internal stresses of martensite for $f = 0.37$ and $f = 0.50$ are much less than the internal stresses of martensite for $f < 0.3$. This is because of the martensite plasticity. It can be concluded that martensite plasticity has an important role in relaxation of the internal stresses.

5. Conclusions

Tensile properties and inhomogeneous deformation of ferrite–martensite dual-phase steels containing 17–50% martensite were analysed. The results are summarized as follows.

1. The stress of dual-phase steels at a strain was proportional to the volume fraction of martensite, f. The slope of σ–f curve ($= d\sigma/df$) has a transition at $f \approx 0.3$; the slopes in the range $0.17 \leqslant f \leqslant 0.27$ were approximately three times as large as those for $0.32 \leqslant f \leqslant 0.50$. This was related to the plastic deformation of martensite.

2. In Jaoul–Crussard analyses, a three-stage deformation was found in the dual-phase steels if $f < 0.3$. This characteristic deformation comes from the three-stage deformation of the ferrite matrix, and it disappears if $f > 0.3$.

3. The newly developed theory showed the relation between the *in situ* stress–strain curves of ferrite, martensite and their composite (dual-phase steel). The theory proved to be an intermediate theory between the iso-stress theory and the iso-strain theory.

4. The stress ratios, $\sigma_{11}^2/\sigma_{11}^1$, increased for low deformation, for larger deformation they were nearly saturated at values between 1.6 and 2.2. For $f > 0.3$, the stress ratios were much reduced by plastic deformation of martensite. Microhardness ratios between ferrite and martensite at uniform strain were also present between 1.6 and 2.2.

5. During deformation the strain ratios, $\varepsilon_{11}^2/\varepsilon_{11}^1$, decreased before yielding of martensite, but they were almost saturated after the yielding of martensite. The variation of strain ratios was very sensitive to the volume fraction and strength of martensite.

6. According to theoretical evaluation, the martensite phase yields after the uniform strain for $f < 0.25$, while it deforms plastically before the uniform strain if $f > 0.25$.

7. The *in situ* stress–strain curves of ferrite and martensite were calculated from the partitioned stresses and strains. Low deformation of ferrite was dependent on the slip distance (mean intercept length) of ferrite, the *in situ* stress–strain curves of martensite, however, were largely dependent on the volume fraction of martensite.

8. Internal stresses at respective phases increased rapidly in the small strain region, and at larger strain the increasing rates were much reduced by plastic relaxation in ferrite and by plastic deformation of martensite.

Appendix

When uniaxial stress, σ, is externally applied to a composite body, the strain energy density is represented as

$$U = \int_0^{\varepsilon} \sigma(\varepsilon')\,d\varepsilon' \tag{A1}$$

where ε is the composite strain. If the flow curve of the composite is given by the form of a Hollomon curve [33];

$$\sigma = K\varepsilon^n \tag{A2}$$

then integration of the strain energy density gives

$$U = \frac{K}{n+1}\varepsilon^{n+1} = \frac{1}{n+1}\sigma\varepsilon. \tag{A3}$$

The composite stress and composite strain can be calculated from the *in situ* stresses and strains of constituent phases by means of the modified rules of mixtures [34]. When the composite consists of two phases and the volume fractions of phase 1 and phase 2 are given by f_1 and f_2, respectively, the modified rules of mixtures are

$$\sigma = f_1\sigma_1 + f_2\sigma_2 \tag{A4}$$

$$\varepsilon = f_1\varepsilon_1 + f_2\varepsilon_2 \tag{A5}$$

where σ_1 and σ_2 are the *in situ* effective stresses at phase 1 and phase 2, respectively, and ε_1 and ε_2 are the *in situ* effective strains at respective phases. Applying Equations A4 and A5 to Equation A3, the strain energy density becomes

$$U = \frac{1}{n+1}\langle f_1\sigma_1 + f_2\sigma_2\rangle\langle f_1\varepsilon_1 + f_2\varepsilon_2\rangle. \tag{A6}$$

A constraint to which the volume fractions are subject is defined by

$$C = f_1 + f_2 - 1 = 0 \tag{A7}$$

The increasing path of the strain energy density during deformation is constrained by the microstructure of the specimen and the loading conditions. The constraints give the minimized or maximized path along which the energy of the system increases. Since we have Equation A7, we shall assume that the strain energy density, U, of Equation A6 has an extreme value during deformation. The Lagrangian-multiplier method [35] is suitable for finding the extreme-value condition. In this method the constraints are incorporated into the increment of a physical quantity by means of multipliers.

Differentiating U and C by f_1 and f_2 gives

$$dU = \frac{\partial U}{\partial f_1}df_1 + \frac{\partial U}{\partial f_2}df_2 \tag{A8}$$

$$dC = \frac{\partial C}{\partial f_1}df_1 + \frac{\partial C}{\partial f_2}df_2 \tag{A9}$$

A Lagrangian multiplier, λ, is introduced to construct the extreme-value condition of U as [13]

$$dU + \lambda dC = 0 \quad \text{(A10)}$$

Inserting Equations A8 and A9 into Equation A10, then

$$\frac{\partial U}{\partial f_1} + \lambda \frac{\partial C}{\partial f_1} = 0 \quad \text{(A11)}$$

$$\frac{\partial U}{\partial f_2} + \lambda \frac{\partial C}{\partial f_2} = 0 \quad \text{(A12)}$$

Since Equation A7 gives the following condition

$$\frac{\partial C}{\partial f_1} = \frac{\partial C}{\partial f_2} = 1 \quad \text{(A13)}$$

one can write

$$\frac{\partial U}{\partial f_1} = \frac{\partial U}{\partial f_2} = -\lambda \quad \text{(A14)}$$

where λ is a constant which need not be determined. When this condition is satisfied, U is an extremum at a stress–strain state.

Inserting Equation A6 into Equation A14

$$2(1-f)\sigma_1\varepsilon_1 + f\sigma_1\varepsilon_2 + f\sigma_2\varepsilon_1 = 2f\sigma_2\varepsilon_2 + (1-f)\sigma_1\varepsilon_2 + (1-f)\sigma_2\varepsilon_1 \quad \text{(A15)}$$

where $f_1 = 1 - f$ and $f_2 = f$. Using the modified rules of mixtures, two governing equations can be derived for inhomogeneous deformation of a two-phase composite from this equation (see Equations 2 and 8 in the text).

References

1. R. G. DAVIES, *Met. Trans.* **9A** (1978) 451.
2. G. R. SPEICH, "Fundamentals of dual-phase Steels", edited by R. A. Kot and B. L. Bramfitt (TMS-AIME, Warrendale, Pennsylvania 1981) 3.
3. R. D. LAWSON, D. K. MATLOCK and G. KRAUSS, *ibid.* 347.
4. K. ARAKI, Y. TANAKA and K. NAKAOKA, *Trans. ISIJ*, **17** (1977) 85.
5. J. GERBASE, J. D. EMBURY and R. M. HOBBS, "Structure and properties of dual-phase steels", edited by R. A. Kot and J. W. Morris (TMS-AIME, New York, 1979) 118.
6. A. F. SZEWCZYK and J. GURLAND, *Met. Trans.* **13A** (1982) 1821.
7. H. P. SHEN, T. C. LEI and J. Z. LIU, *Mater. Sci. and Tech.* **2** (1986) 28.
8. Y. L. SU and J. GURLAND, *Mater. Sci. and Engng.* **95** (1987) 151.
9. D. V. WILSON and Y. A. KONNAN, *Acta Metall.* **12** (1964) 617.
10. Y. W. CHANG and R. J. ASARO, *Mater. Sci.* **12** (1978) 277.
11. P. S. BATE and D. V. WILSON, *Acta Metall.* **34** (1986) 1097.
12. K. CHO and J. GURLAND, *Met. Trans.* **19A** (1988) 2027.
13. T. S. BYUN and I. S. KIM, *J. Mater. Sci.* **26** (1991) 3917.
14. Y. TOMOTA, K. KUROKI, T. MORI and I. TAMURA, *Mater. Sci. and Engng.* **24** (1976) 85.
15. J. C. FISHER, E. W. HART and R. H. PRY, *Acta Metall.* **1** (1953) 336.
16. J. D. ESHELBY, *Proc. Roy. Soc. A* **241** (1957) 376.
17. *Idem., ibid.* **252** (1959) 561.
18. K. TANAKA and T. MORI, *Acta Metall.* **18** (1970) 931.
19. L. M. BROWN and W. M. STOBBS, *Phil. Mag.* **23** (1971) 1185.
20. L. M. BROWN, *Acta Metall.* **21** (1973) 893.
21. L. M. BROWN and D. R. CLARKE, *ibid.* **23** (1975) 221.
22. M. F. ASHBY. *Phil. Mag.* **14** (1966) 1157.
23. *Idem., ibid.* **21** (1970) 399.
24. F. J. HUMPHREYS and J. W. MARTIN, *ibid.* **16** (1967) 927.
25. P. F. CHAPMAN and W. M. STOBBS, *ibid.* **19** (1969) 1015.
26. L. M. BROWN and W. M. STOBBS, *ibid.* **23** (1971) 1201.
27. R. W. K. HONEYCOMBE, *Trans. ISIJ*, **20** (1980) 139.
28. J. GURLAND, *Mater. Sci. and Engng.* **40** (1979) 59.
29. B. JAOUL, *J. Mech. Phys. Sol.* **5** (1957) 95.
30. W. C. LESLIE and R. J. SOBER, *Trans. Am. Soc. Met.* **60** (1967) 459.
31. W. C. LESLIE, "The physical metallurgy of steels", (McGraw-Hill, New York, 1981) 217.
32. G. KRAUSS, "Principles of heat treatment of steel", (American Society of Metals, Metals Park, Ohio, 1980) p. 8.
33. J. H. HOLLOMON, *Trans. TMS-AIME*, **62** (1945) 268.
34. H. FISCHMEISTER and B. KARLSSON, *Z. Metallkunde*, **68** (1977) 311.
35. G. ARFKEN, "Mathematical methods for physicists", 2nd edn (Academic Press, New York 1982) 790.

Received 16 January
and accepted 26 October 1992